Journal of
Ceramic Science
and Technology

J. Ceram. Sci. Technol., **13** [2] 99-106 (2022)
DOI: 10.4416/JCST2022-00001
available online at: http://www.ceramic-science.com

Improved Flexural Strength in Digital-Light-Processing-Printed Si_3N_4 Ceramics by Removing Carbon Residue

B. Jin[1], Y. Bian[1], Y. Shen[1], B. Xing[1], M. Li[2], Z. Zhao[*1]

[1]School of Materials Science and Engineering, Shanghai Institute of Technology, Shanghai, 201418, China
[2]Jiaxing CeramPlus Technology Co., Ltd., Jiaxing, 314100, China

received January 7, 2022; received in revised form April 28, 2022; accepted May 5, 2022

Abstract

The debinding step is vitally important to obtain defect-free ceramics in the fabrication of ceramics by means of DLP-3D printing. However, the residual carbon from the decomposition of the organic matter during the debinding process severely affects the quality and mechanical properties of the sintered ceramics. In this work, it has been proven that the carbon residue can participate in a carbothermal reduction reaction at 1 300 °C and lead to the formation of macroscopic defects such as delamination and cracks that occurred in the surface of the sintered silicon nitride ceramics. Based on this, we propose an approach to eliminate the carbon retained in silicon nitride compacts fabricated with the stereolithography technique. The amount of carbon residue that remained in the debinded silicon nitride bodies is 0.58 % based on thermogravimetric analysis in air atmosphere. When the oxidation temperature and holding time in the air were 450 °C and 5 h, respectively, the residual carbon in the samples could be sufficiently removed. The flexural strength of sintered ceramics without the removal of carbon residue is only 184.88 ± 8.16 MPa; sintered silicon nitride ceramics after removal of residual carbon can reach 469.78 ± 11.86 MPa. The research results in this study provide great reference value for the preparation of defect-free ceramics.

Keywords: *Silicon nitride ceramics, DLP, residual carbon, flexural strength*

I. Introduction

Structural ceramics based on silicon nitride (Si_3N_4) offer excellent mechanical properties, outstanding thermal shock resistance, good chemical resistance and dielectric properties [1,2]. They have been widely applied in mechanical, electronic, biomedical, and aerospace applications [3–6]. To meet certain relatively strict and specific requirements in some areas, multifarious ceramic shaping methods are utilized to produce Si_3N_4 ceramics that remain stable for decades (injection molding, slip casting, and tape casting) [7–10]. However, these conventional ceramic shaping techniques are limited when it comes to high-efficiency production of ceramic components with complex shapes. They are costly on account of the use of expensive molds, long production times, and challenging post-machining after sintering, which limits the applications of Si_3N_4 ceramics [11].

3D printing, also known as additive manufacturing (AM) technology, can solve the problems associated with complex shape. AM has tremendous potential to quickly fabricate high-precision ceramic parts with arbitrarily designed structures without any molds. This greatly enhances production efficiency for the manufacturing industry [12,13]. To date, several AM techniques, such as selective laser sintering (SLS), direct ink writing (DIW), fused deposition modeling (FDM), and digital light processing (DLP), have been developed and used to prepare ceramic materials.

* Corresponding author: zhezhao@kth.se

DLP is a relatively mainstream AM technology and has been widely used to fabricate structural ceramics owing to its high molding accuracy, high efficiency, and low cost [14]. DLP utilizes ultraviolet light illuminated by a projector to selectively project an integral image on a photocurable liquid slurry surface, on which the photosensitive resin is solidified and tightly binds the ceramic powder under the influence of UV light with a specific wavelength [15]. This process is repeated until the desired ceramic green body object is obtained. The photopolymerizable ceramic suspensions also contain a dispersant, a photoinitiator, and a photosensitive resin. After the printing step, the resulting ceramic green body can be subjected to a suitable thermal debinding process to burn out the organic binders at high temperatures and is then densified in the subsequent sintering process [16]. DLP offers a new route to control the performance of Si_3N_4 ceramics based on a diversified structure design.

During the polymerization of ceramic slurries, the introduction of ceramic particles significantly reduces the curing properties of the photosensitive resin because of the particles' light scattering; this is especially relevant for ceramic materials with a large refractive index (RI) [17,18]. A larger RI lowers the cure depth (C_d) of the ceramic suspension and reduces the dimensional resolution during printing. This is detrimental to the fabrication of ceramic components with high surface quality [19,20]. Therefore, the main obstacle in forming Si_3N_4 ceramics by means of

DLP-3D printing is the large RI (n = 2.1) of Si_3N_4 ceramic particles [21]. The larger absorption of Si_3N_4 particles also severely impairs their curing performance, making it difficult to shape Si_3N_4 green parts by means of polymerization-based AM technology [22]. Thus, previous studies have primarily focused on enhancing the curing properties of Si_3N_4 ceramic suspensions via the treatment of the powder surface based on optimization of the slurry formulation. Dense Si_3N_4 ceramics with complex-shapes have been successfully prepared [23–25]. While problems involving molding Si_3N_4 by stereolithography have been effectively addressed, very few researchers have studied the importance of carbonaceous residue left behind during debinding [26]. In contrast to oxide ceramics, the carbon residue in Si_3N_4 brown bodies cannot be decomposed because the silicon nitride must be sintered under a nitrogen atmosphere (the protective gas prevents oxidation) [27].

This research aims to eliminate the residual carbon generated during the debinding step for DLP-printed Si_3N_4 ceramics. Silicon nitride ceramic bodies were fabricated by means of stereolithography-based 3D printing. The printed samples were then subjected to the same thermal debinding conditions and sintered at different temperatures under a nitrogen atmosphere. The effect of the debinding temperature on the mechanical properties and the microstructure of silicon nitride ceramics was thus investigated. The residual carbon in the ceramic samples was detected and then completely removed. The effect of the carbon residue on the macromorphology and the mechanical properties of sintered ceramics was also investigated based on controls without residual carbon. The findings can lead to non-oxide ceramics without cracks prepared via stereolithography.

II. Experimental

(1) Fabrication of silicon nitride samples

This work used a silicon nitride ceramic slurry with a solid load of 45 vol% and a commercial 3D printer from Jiaxing CeramPlus Tech. Co. LTD. (Zhejiang Province, China). The wavelength of the UV light in the DLP stereolithography printer was 385 nm from a light-emitting diode (LED). To promote liquid-phase sintering and achieve densification, 10 wt% yttria-alumina (Y_2O_3-Al_2O_3) with a mass ratio of 2:1 was added into the silicon nitride photosensitive slurry. After the sintering aids were added, the resulting slurry was ball-milled for 24 h at 360 rpm to ensure uniform distribution of ceramic powder in a photocurable resin. The ball-milled ceramic slurry was then transferred to a printer tank to prepare silicon nitride ceramic samples. During printing, the layer thickness was 25 μm, the exposure time was 8 s, and the exposure energy was 40 mW/cm^2. The silicon nitride green bodies measured 35 × 4 × 3 mm after printing and were then washed with ethanol to remove residual slurry on the surface of the samples.

(2) Debinding and sintering

The as-prepared green bodies were debinded in an atmosphere furnace (GF17Q, Nanjing Boyuntong Instrument Technology Co., China) under a nitrogen atmosphere. Nitrogen debinding can effectively prevent severe thermal pyrolysis and gasification of the cured resin in the printed sample [28]. The debinding temperature profile is illustrated in Fig. 1(a). Heating rates of 1 K/min and 0.25 K/min were chosen for the temperature ranges of RT – 150 °C and 150 – 600 °C, respectively. They were then ramped to 1 000 °C, 1 100 °C, 1 200 °C, and 1 300 °C at 2 K/min and held for 2 h. These samples were denoted S-1000, S-1100, S-1200, and S-1300. The samples were then transferred to a sintering furnace (GSP120, Shanghai Chenrong Instrument Technology Co., China) for sintering with nitrogen as a protective atmosphere at 4 MPa applied gas pressure. The sintering profile is illustrated in Fig. 1(b).

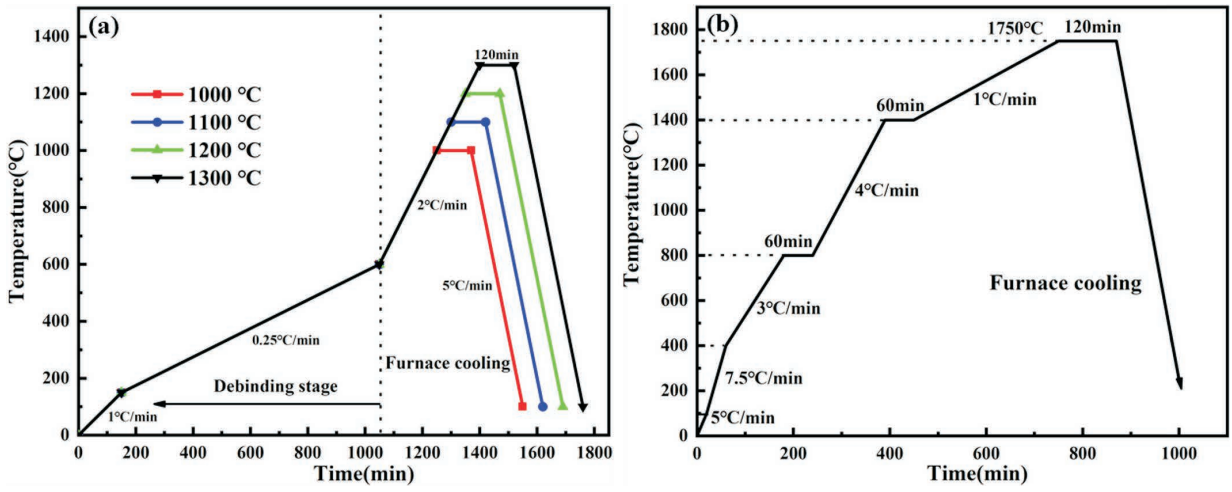

Fig. 1: Debinding (a) and (b) sintering profile of green bodies.

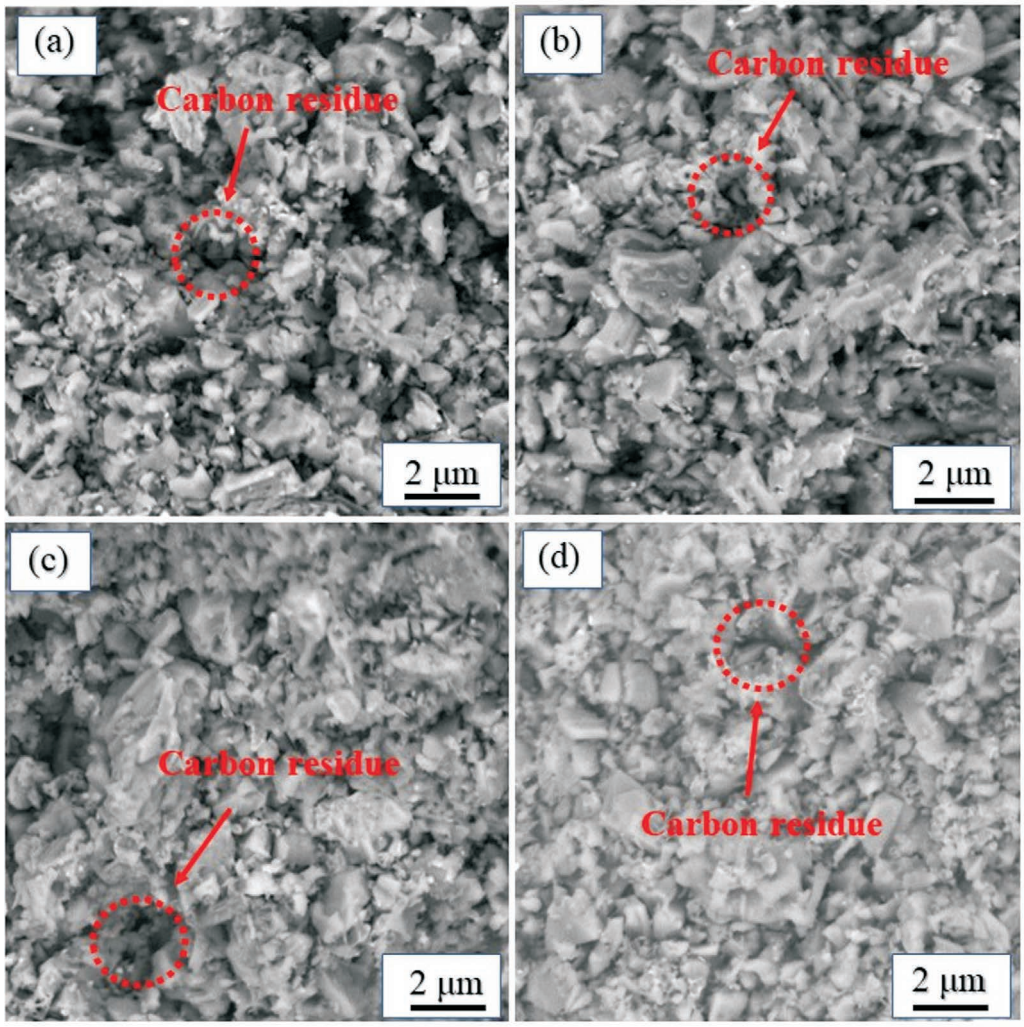

Fig. 3: SEM images of the fracture surface of silicon nitride ceramics debinded at different temperatures: (a) 1 000 °C, (b) 1 100 °C , (c) 1 200 °C, and (d) 1 300 °C.

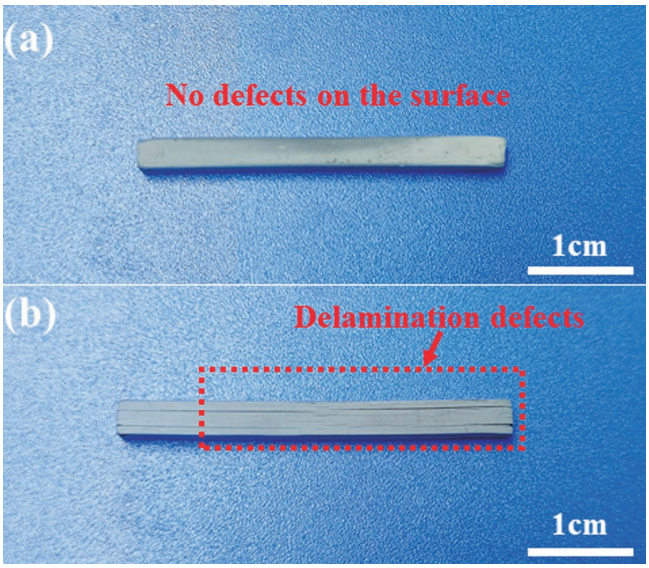

Fig. 4: Side view of the Si_3N_4 ceramics debinded at different temperatures: (a) 1 200 °C ; (b) 1 300 °C.

Hu *et al.* [35] have reported that the introduction of a small amount of carbon can react with the grain boundary glass phase and nitrogen during post-sintering heat treatment, thus leading to a significant improvement in the thermal conductivity of Si_3N_4 ceramics. Thus, we concluded that the formation of cracks on the surface of the sample S-1300 can probably be attributed to rapidly expanding CO gas owing to the carbothermal reduction that occurred at the higher sintering temperature. Here, residual carbon can react via SiO_2 under a reducing N_2 atmosphere. The presence of residual carbon elements resulting from carbonization of the cured resin in nitrogen during the low-temperature debinding stage does not enhance the sintering properties of Si_3N_4 ceramics because the generation of cracks is fatal in ceramics. Therefore, any residual carbon should be eliminated as soon as possible to ensure densification and maintain the mechanical properties of the sintered ceramics.

Thermogravimetric analysis (TGA) in air was used to determine the content of the residual carbon in S-1200 and the result is shown in Fig. 5. The weight loss of the sample decreased sharply from room temperature to 99.8 °C with a mass loss of 0.41 %. The weight loss was mainly because of the evaporation of water absorbed in air [15]. As the oxidation temperature increased, a maximum mass loss of 0.99 % was obtained at 461.6 °C. We concluded that

the practical weight loss was nearly 0.58 %. This suggests that this value should be a good indicator of the carbon residue that remained in S-1200. The mass of the sample began to increase when the oxidation temperature exceeded 461.6 °C, thus illustrating that the entire carbon residue in S-1200 decomposed at this temperature, and SiO_2 gradually formed via oxidation to improve sample quality.

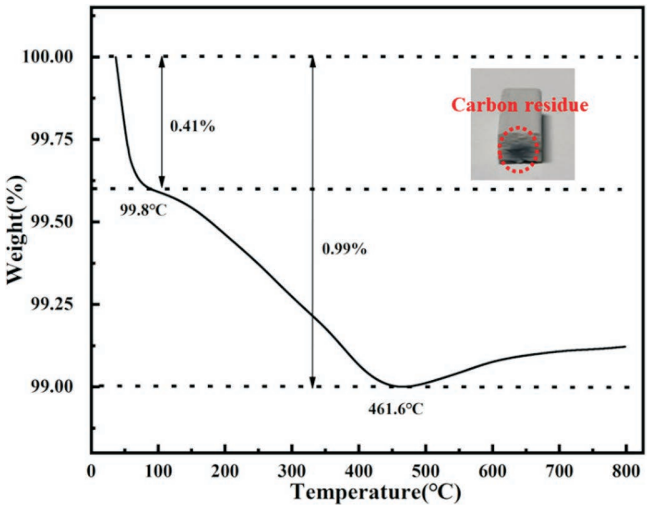

Fig. 5: Thermogravimetric analysis curves of the Si_3N_4 debinded body.

This analysis led to a method for removing residual carbon. Low-temperature oxidation in the air is an effective way to reduce the content of carbon remaining in sintered ceramics [36, 37]. The highest oxidation temperature for eliminating carbon was set to 450 °C to avoid significant formation of SiO_2 on the surface of the Si_3N_4 particles. Sample S-1200 was used as an example and then oxidized at different temperatures (300 °C – 450 °C) with the same heating rate of 5 K/min and dwelling time of 2 h, to evaluate the effect of the oxidation temperature on the efficiency of carbon removal. The fracture morphology of S-1200 oxidized at different temperatures is shown in Fig. 6. The residual carbon was present in the form of debris at 300 °C and 350 °C. Little carbon is left at 400 °C and 450 °C; thus, the oxidation temperature should be over 400 °C.

Fig. 7 shows the bulk density of S-1200 as a function of the oxidation temperature for 2 h. The density decreased to 2.18 g/cm^3 when the oxidation temperature increased from 300 °C to 450 °C. This can be explained by the carbon's removement in the sample heated at a higher oxidation temperature, at which the carbon was more easily decomposed in the air; a portion of CO_2 was thus produced from inside to outside. Furthermore, there are no cracks generated on the surface of all sintered samples after oxidation, suggesting that the oxidation reaction corresponding

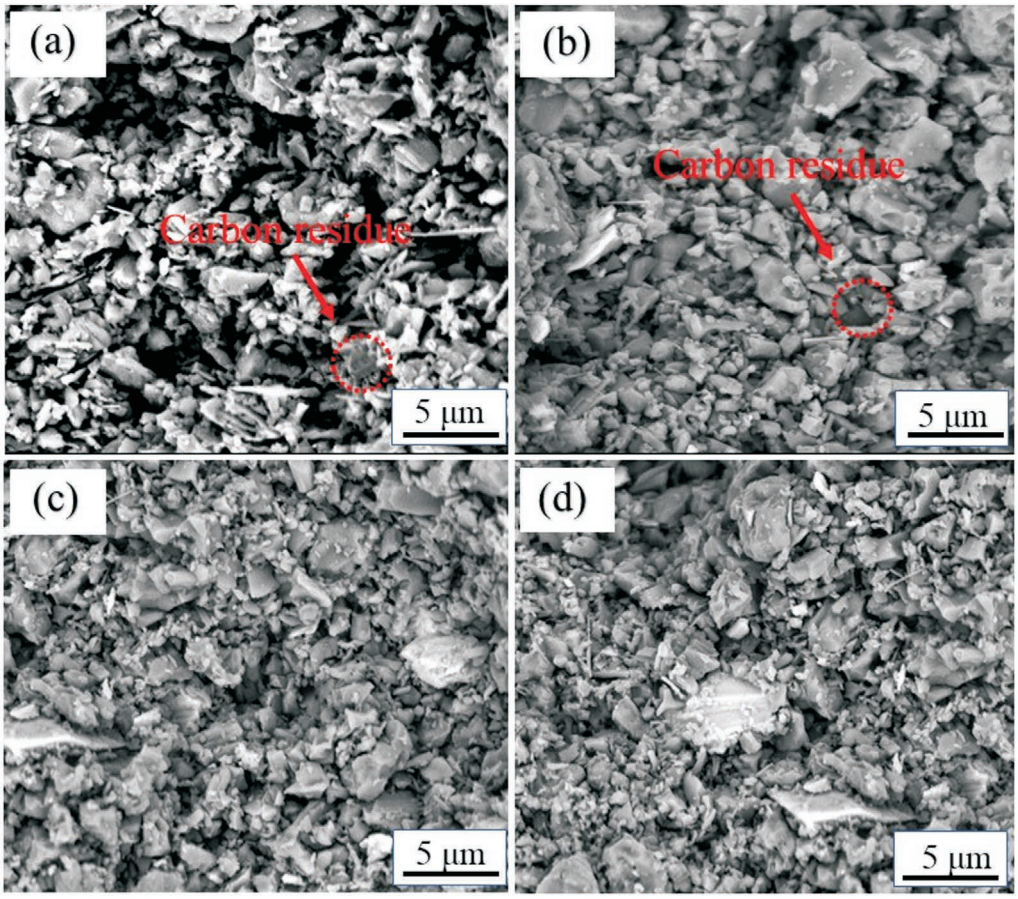

Fig. 6: SEM images of the fracture surface of sample S-1200 oxidized at: (a) 300 °C , (b) 350 °C, (c) 400 °C, and (d) 450 °C.

to these temperatures was relatively mild and the resulting CO_2 wasdegassed smoothly from the ceramic green part. This leads to favorable sintering. Thus, 450 °C was selected to remove carbon for further use of the materials.

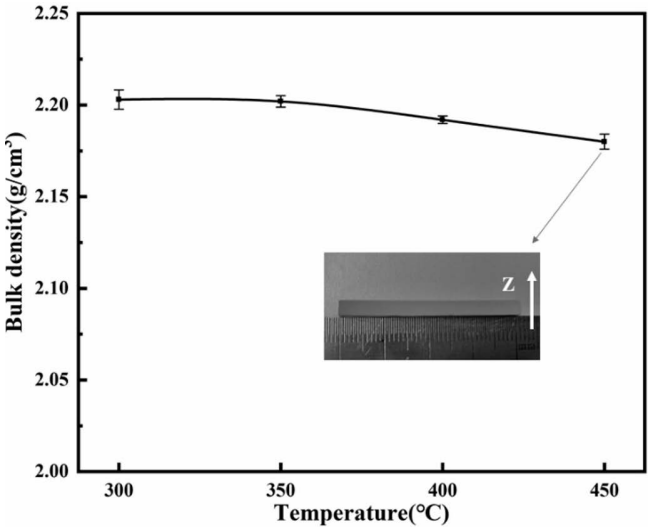

Fig. 7: Bulk density of Si_3N_4 debinded bodies as a function of oxidation temperature.

The holding time at 450 °C in air was also evaluated with regard to the removal of carbon residue. The weight loss of the sample as a function of the holding time is shown in Fig. 8. With increasing holding time, the weight loss of the sample decreased markedly and then remained constant at times over 5 h, suggesting that the residual carbon remaining in the sample had been adequately oxidized. Thus, the optimal holding time selected here for eliminating carbon residue at 450 °C in air is 5 h.

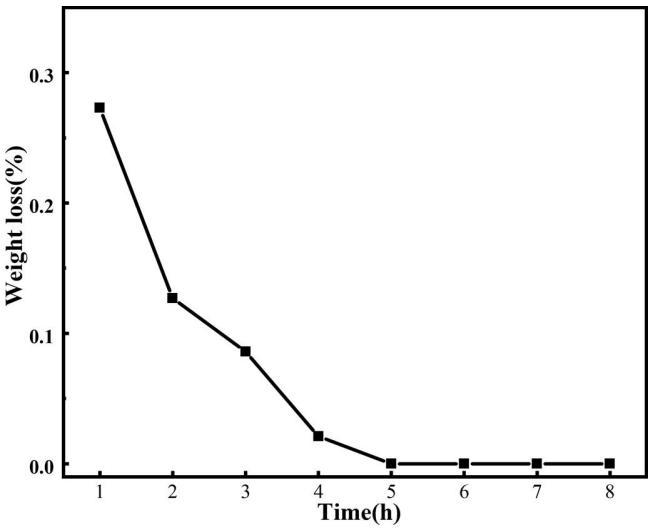

Fig. 8: Weight loss of the debinded samples oxidized at 450 °C in air as a function of holding time.

To verify this strategy, the following experiments were performed. Samples that had been debinded at 1 200 °C were divided into two groups: One group was left untreated, and the other group was heated to 450 °C and held for 5 h in air (SN-1 and SN-2, respectively). All samples were then sintered at 1 750 °C based on the sintering profile illustrated in Fig. 1(b). Optical microscopy data of the sintered ceramics, without and with the removal of residual carbon, are shown in Fig. 9(a) and (b), respectively. Severe deformation and obvious cracks are seen on the ceramic sample without oxidation treatment before sintering. There are no visible defects on the sintered sample with oxidation treatment. This proves that the small amount of residual carbon due to insufficient pyrolytic activity can participate in carbothermal reactions and lead to fatal defects.

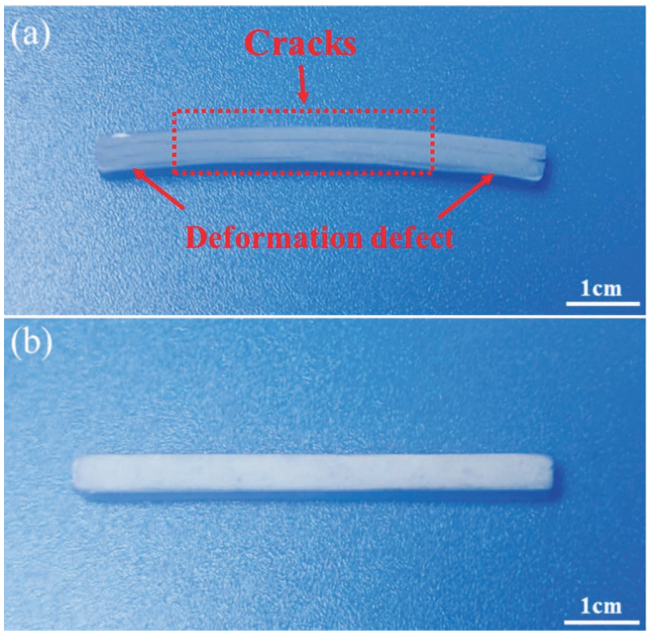

Fig. 9: Side view of sintered Si_3N_4 ceramic without (a) removal of carbon, with (b) removal of carbon.

The mechanical properties of the sintered Si_3N_4 ceramics with and without carbon residue are shown in Table 1. The relative density of all sintered samples is slightly lower, which is probably explained by the low sintering temperature (1 750 °C). The sintered ceramic samples from which the carbon residue has been removed show excellent flexural strength up to 469.78 ± 11.86 MPa, which is more than double the strength of the samples without removal of carbon residue. These data indicate that the flexural strength of ceramics can be remarkably improved thanks to the removal of carbon residue.

Table 1: Mechanical properties of the sintered Si_3N_4 ceramics without (SN-1) and with (SN-2) removal of carbon residue.

	Relative density (%)	Flexural strength (MPa)
SN-1	87.40	184.88 ± 8.16
SN-2	90.49	469.78 ± 11.86

The variation in flexural strength of sintered silicon nitride ceramics is usually determined based on the microstructural evolution. Fig. 10(a) shows the microstructure of the sintered Si_3N_4 ceramics without removal of

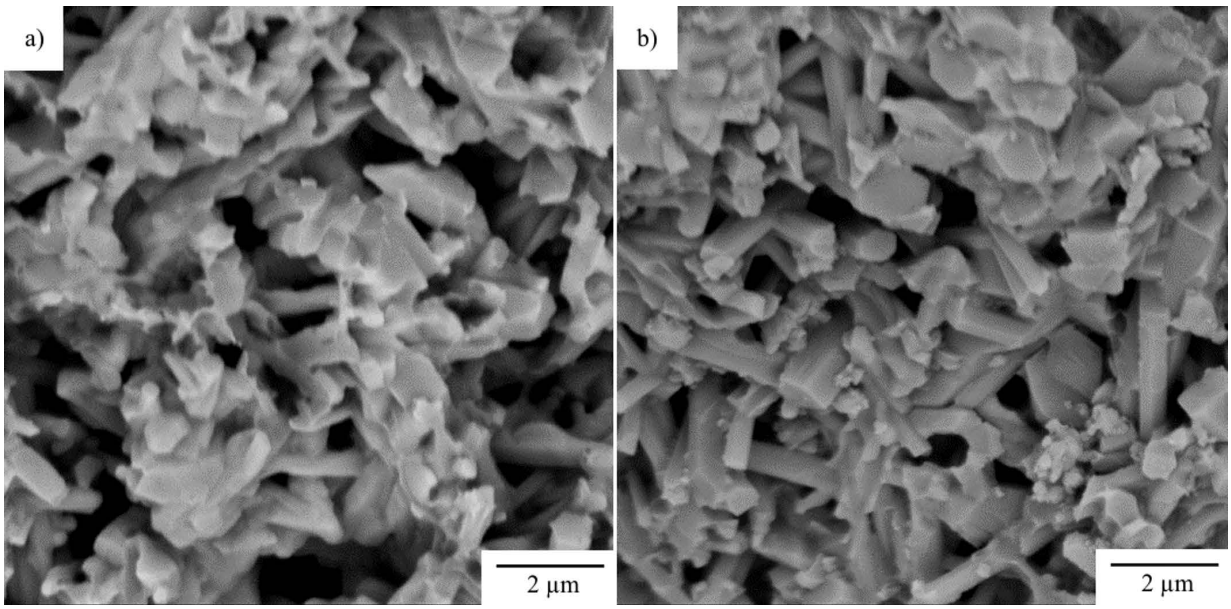

Fig. 10: SEM micrographs of the fracture surface of (a) SN-1, and (b) SN-2.

carbon residue. The number of rod-shaped β-Si_3N_4 granules with a high aspect-ratiowas relatively limited, perhaps because residual carbon reduced the content of SiO_2 owing to carbothermal reduction at high sintering temperatures, thus leading to the formation of less liquid, which in turn restricts anisotropic grain growth of β-Si_3N_4 nuclei [34]. Many pores were present in the sample, leading to low flexural strength and densification. Fig. 10(b) shows the morphology of sintered Si_3N_4 ceramics after the removal of residual carbon. Although pores are present between the granules, many columnar grains with high aspect ratios are also visible, suggesting that the transformation of α-Si_3N_4 to β-Si_3N_4 is complete. These β-Si_3N_4 overlapped tightly with each other and were distributed on some of the Si_3N_4 grains, thus greatly enhancing the flexural strength of the sintered Si_3N_4 ceramics.

IV. Conclusions

Silicon nitride green bodies were fabricated using a DLP 3D printing technology. The influence of the debinding temperature on the mechanical properties and microstructure of the debinded ceramic samples was investigated. The flexural strength of the debinded silicon nitride bodies peaked at 18.5 ± 0.75 MPa when the debinding temperature was 1 300 °C. The residual carbon that remained in the ceramics was identified and eliminated by means of low-temperature oxidation treatment. At an oxidation temperature and holding time in the air of 450 °C and 5 h, respectively, the carbonaceous products left after the debinding step were removed sufficiently. The sintered silicon nitride ceramics without removal of the carbon residue exhibited a flexural strength of 184.88 ± 8.16 MPa. The silicon nitride ceramics without residual carbon can reach 469.78 ± 11.86 MPa. This indicates that although the content of carbon residue is relatively small, it has a considerable impact on the mechanical properties and densification of the sintered silicon nitride ceramic parts. Residual carbon must be eliminated to fabricate fully dense silicon nitride ceramic parts with high strength.

Acknowledgements

This work was supported by the National Key R&D Program of China (Nos. 2017YFB1103500 and 2017YFB1103502), Shanghai Technical Service Center for Advanced Ceramics Structure Design and Precision Manufacturing (NO. 20DZ2294000) and the Key Research and Development Projects in Zhejiang Province (NO. 2021C01SA403330).

References

1 Krstic, Z., Krstic, V.D.: Silicon nitride: the engineering material of the future, *J. Mater Sci.*, **47**, 535 – 552, (2012).

2 Ohji, T.: Microstructural design and mechanical properties of porous silicon nitride ceramics, *Mater. Sci. Eng.*, **498**, 5 – 11, (2008).

3 Ding, S., Zeng, Y.P., Jiang, D.: Oxidation bonding of porous silicon nitride ceramics with high strength and low dielectric constant, *Mater. Lett.*, **61**, 2277 – 2280, (2007).

4 Lu, H., Bailey, C., Yin, C.: Design for reliability of power electronics modules, *Microelectron. Reliab.*, **49**, 1250 – 1255, (2009).

5 Webster, T.J., Patel, A.A., Rahaman, M.N., Sonny Bal, B.: Anti-infective and osteointegration properties of silicon nitride, poly (ether ether ketone), and titanium implants, *Acta Biomater.*, **8**, 4447 – 4454, (2012).

6 Zhang, J.,Chen, J.W., Wang, H.J.: High performance porous wave-transmitting silicon nitride ceramics by gel-casting technique, *Key Eng. Mater.*, **512**, 869 – 872, (2012).

7 Rueschhoff, L.M., Trice, R.W., Youngblood, J.P.: Near-net shaping of silicon nitride via aqueous room-temperature injection molding and pressureless sintering, *Ceram. Int.*, **43**, 10791 – 10798, (2017).

8 Zou, C., Guo, S., Zhou, X., Li, S., Yan, C., Shen, T.: Gel-casting prepared porous Si_3N_4 ceramics with different contents of Y_2O_3 and Al_2O_3 additives, *J. Mater. Eng. Perform.*, **29**, 7891 – 7898, (2020).

9 Studart, A.R., Gonzenbach, U.T., Tervoort, E., Gauckler, L.J.: Processing routes to macroporous ceramics: a review, *J. Am. Ceram. Soc.*, **89**, 1771 – 1789, (2006).

10 Yang, X., Li, B., Zhang, C., Wang, S., Liu, K., Zou, C.: Fabrication and properties of porous silicon nitride wave-transparent ceramics via gel-casting and pressureless sintering, *Mater. Sci. Eng.*, **663**, 174 – 180, (2016).

11 Altun, A.A., Prochaska, T., Konegger, T., Schwentenwein, M.: Dense, strong, and precise silicon nitride-based ceramic parts by lithography-based ceramic manufacturing, *Appl. Sci.*, **10**, 996, (2020).

12 Ryan, K.R., Down, M.P., Banks, C.E.: Future of additive manufacturing: overview of 4D and 3D printed smart and advanced materials and their applications, *Chem. Eng. J.*, **403**, 126162, (2021).

13 Hwa, L.C., Rajoo, S., A.M. Noor, N. Ahmad, M.B. Uday: Recent advances in 3D printing of porous ceramics: A review, *Curr. Opin. Solid State Mater. Sci.*, **21**, 323 – 347, (2017).

14 G. Ding, R. He, K. Zhang, M. Xia, C. Feng, D. Fang: Dispersion and stability of SiC ceramic slurry for stereolithography, *Ceram. Int.*, **46**, 4720 – 4729, (2020).

15 Shen, M., Zhao, W., Xing, B., Sing, Y., Gao, S., Wang, C., Zhao, Z.: Effects of exposure time and printing angle on the curing characteristics and flexural strength of ceramic samples fabricated via digital light processing, *Ceram. Int.*, **46**, 24379 – 24384, (2020).

16 Schmidt, J., Colombo, P.: Digital light processing of ceramic components from polysiloxanes, *J. Eur. Ceram. Soc.*, **38**, 57 – 66, (2018).

17 Zakeri, S., Vippola, M., Levänen, E.: A comprehensive review of the photopolymerization of ceramic resins used in stereolithography, *Addit. Manuf.*, **35**, 101177, (2020).

18 Tomeckova, V., Halloran, J.W.: Predictive models for the photopolymerization of ceramic suspensions, *J. Eur. Ceram. Soc.*, **30**, 2833 – 2840, (2010).

19 Chen, Z., Li, J., Liu, C., Liu, Y., Zhu, J.Lao, C.: Preparation of high solid loading and low viscosity ceramic slurries for photopolymerization-based 3D printing, *Ceram. Int.*, **45**, 11549 – 11557, (2019).

20 Rasaki, S.A., Xiong. D., Xiong, S., Su, F.,Idrees, M., Chen, Z.: Photopolymerization-based additive manufacturing of ceramics: A systematic review, *J. Adv. Ceram.*, **10**, 442 – 471, (2021).

21 Hinczewski, C., Corbel, S., Chartier, T.: Ceramic suspensions suitable for stereolithography, *J. Eur. Ceram. Soc.*, **18**, 583 – 590, (1998).

22 Li, X., Zhang, J., Duan, Y., Liu, N., Jiang, J.: Rheology and curability characterization of photosensitive slurries for 3D printing of Si_3N_4 ceramics, *Appl. Sci.*, **10**, 6438, (2020).

23 Huang, R.J., Jiang, Q.G., Wu, H.D.: Fabrication of complex shaped ceramic parts with surface-oxidized Si_3N_4 powder via digital light processing based stereolithography method, *Ceram. Int.*, **45**, 5158 – 5162, (2019).

24 Liu, Y., Zhan, L., He, Y.U., Zhang, J: Stereolithographical fabrication of dense Si_3N_4 ceramics by slurry optimization and pressure sintering, *Ceram. Int.*, **46**, 2063 – 2071, (2020).

25 Wu, X., Xu, C., Zhang, Z.: Preparation and optimization of Si_3N_4 ceramic slurry for low-cost LCD mask stereolithography, *Ceram. Int.*, **47**, 9400 – 9408, (2021).

26 He, R., Liu, W., Wu, Z., An, D.: Fabrication of complex-shaped zirconia ceramic parts via a DLP-stereolithography-based 3D printing method, *Ceram. Int.*, **44**, 3412 – 3416, (2018).

27 Bocanegra-Bernal, M.H., Matovic, B.: Dense and near-net-shape fabrication of Si_3N_4 ceramics, *Mater, Sci. Eng.*, **500**, 130 – 149, (2009).

28 Zhang, J., Wei, L., Meng, X., Yu, F., Yang, N., Liu, S.: Digital light processing-stereolithography three-dimensional printing of yttria-stabilized zirconia, *Ceram. Int.*, **46**, 8745 – 8753, (2020).

29 Li, H., Liu, Y., Liu, Y., Zeng, Q.: Influence of debinding holding time on mechanical properties of 3D-printed alumina ceramic cores, *Ceram. Int.*, **47**, 4884 – 4894, (2021).

30 Ryshkewitch, E.: Compression strength of porous sintered alumina and zirconia: 9th communication to ceramography, *J. Am. Ceram. Soc.*, **36**, 65 – 68, (1953).

31 Li, H., Liu, Y., Liu, Y., Zeng, Q., Hu, K.: Effect of debinding temperature under an argon atmosphere on the microstructure and properties of 3D-printed alumina ceramics, *Mater. Charact.*, **168**, 110548, (2020).

32 Higgins, R.J., Rhine, W.E., Cima, M.J.: Ceramic surface reactions and carbon retention during non-oxidative binder removal Al_2O_3/Poly (methyl methacrylate) at 20 – 700 °C, *J. Am. Ceram. Soc.*, **77**, 2243 – 2254, (1994).

33 Wang, K., Qiu, M., Jiao, C., Gu J., Xie, D.: Study on defect-free debinding green body of ceramic formed by DLP technology, *Ceram. Int.*, **46**, 2438 – 2446, (2020).

34 Li, Y., Kim, H.N., Wu, H.: Enhanced thermal conductivity in Si_3N_4 ceramic by addition of a small amount of carbon, *J. Eur. Ceram. Soc.*, **39**, 157 – 164, (2019).

35 Hu, F., Zhu, T., Xie, Z., Liu, J.: Elimination of grain boundaries and its effect on the properties of silicon nitride ceramics, *Ceram. Int*., **46**, 12606 – 12612, (2020).

36 Zhou, M., Liu, W., Wu, H.: Preparation of a defect-free alumina cutting tool via additive manufacturing based on stereolithography – optimization of the drying and debinding processes, *Ceram. Int.*, **42**, 11598 – 11602, (2016).

37 Wang, K., Bao, C., Zhang, C.: Preparation of high-strength Si_3N_4 antenna window using selective laser sintering, *Ceram. Int.*, **47**, 31277 – 31285, (2021).